Identification of a boron nitride nanosphere-binding peptide for the intracellular delivery of CpG oligodeoxynucleotidess

Huijie Zhang[a,b], Tomohiko Yamazaki[a,b], Chunyi Zhi[b], and Nobutaka Hanagata[a,b,c*]

[a]Graduate School of Life Science, Hokkaido University, N10W8, Kita-ku, Sapporo, 060-0812, Japan
[b]Biomaterials Unit, International Center for Materials Nanoarchitectonics (MANA), National Institute for Materials Science (NIMS), 1-2-1 Sengen, Tsukuba, Ibaraki 305-0047, Japan
[c]Nanotechnology Innovation Station, NIMS, 1-2-1 Sengen, Tsukuba, Ibaraki 305-0047, Japan

[*]To whom correspondence should be addressed. Nanotechnology Innovation Station, National Institute for Materials Science, 1-2-1 Sengen, Tsukuba, Ibaraki 305-0047, Japan; E-mail: HANAGATA.Nobutaka@nims.go.jp; Tel: +81-29-860-4774; Fax: +81-29-859-2475

Abstract

CpG oligonucleotides (CpG ODNs) interact with Toll-like receptor 9 (TLR9), which results in the induction of immunostimulatory cytokines. We delivered CpG ODNs intracellularly using boron nitride nanospheres (BNNS). To enhance the loading capacity of CpG ODNs on BNNS, we used phage display technique to identify a 12-amino acid peptide designated as BP7, with specific affinity for BNNS, and used it as a linker to load CpG ODNs on BNNS. The tyrosine residue (Y) at the eighth position from the N-terminus played a crucial role in the affinity of BP7 to BNNS. BNNS that bound BP7 (BNNS/BP7) were taken up into cells and showed no cytotoxicity, and CpG ODNs were successfully crosslinked with BP7 to create BP7–CpG ODNs conjugates. Using BP7 as a linker, the loading efficiency of CpG ODNs on BNNS increased 5-fold compared to the direct binding of CpG ODNs to BNNS. Furthermore, the BP7–CpG ODNs conjugates–loaded BNNS had a greater capacity to induce interleukin-6 (IL-6) and tumor necrosis factor-alpha (TNF-α) production from peripheral blood mononuclear cells (PBMCs) than that of CpG ODNs directly loaded on BNNS. The higher amount of cytokine induction from BP7–CpG ODNs conjugates–loaded BNNS may be attributed to a higher loading capacity and stronger binding to BNNS with the linker BP7. The greater functionality of BP7-conjugated CpG ODNs on BNNS expands the potential of BNNS for drug delivery applications.

Keywords: CpG oligodeoxynucleotides, drug delivery, boron nitride nanospheres, phage display, peptide

1. Introduction

Bacterial and viral DNA containing unmethylated cytosine-guanine (CpG) dinucleotides stimulate the mammalian innate immune system.[1-4] This process is mediated by the activation of Toll-like receptor 9 (TLR9), a member of Toll-like receptor family.[1, 5-6] CpG oligodeoxynucleotides (CpG ODNs) are short, synthetic, single-stranded DNA sequences containing CpG motifs, which possess a similar immunostimulatory property to bacterial DNA.[3, 7] As such, CpG ODNs delivery has potential for clinical applications in the treatment of infectious diseases, allergies, and cancers.[8-11] However, the immunostimulatory effects are often limited by the poor stability and cellular uptake of CpG ODNs. Chemical modification of nucleotides is an effective technique to protect against degradation by nucleases.[12-14] Nuclease-resistant CpG ODNs consisting of phosphorothioate backbones have been developed by modifying the phosphate group of the nucleic acid targeted by nucleases, replacing the oxygen with sulfur. However, there is concern over undesirable side effects associated with the use of CpG ODNs with a phosphorothioate backbone.[15-17] Since CpG ODNs are negatively charged, it is difficult for them to bind to the negatively charged cell surface. This electrostatic repulsion is believed to limit the efficiency of CpG ODNs uptake. Delivery of unmodified CpG ODNs using carrier nanoparticles is, therefore, one strategy to improve stability and to enhance cellular uptake.[18-22]

With its novel properties and structural similarity to carbon, boron nitride (BN) has received considerable scientific interest, with applications ranging from composite materials to electrical and optical devices.[23-26] Furthermore, BN has the advantage of a high biocompatibility, with easier cellular uptake and lower toxicity than carbon.[27-29] Chen et al. demonstrated passive adsorption of single-stranded DNA oligomers onto the surface of BN nanotubes (BNNT) and cellular uptake of BNNT loaded with the DNA.[27] We previously studied the effect of unmodified CpG ODNs delivery using 150-nm BN nanospheres (BNNS), synthesized by chemical vapor deposition,[30] on TLR9 activation.[31] BNNS had no cytotoxicity, and protected unmodified CpG ODNs from degradation by serum nucleases. In addition, BNNS taken up by cells localized to endolysosomes, and this localization was maintained even after cell division; this was particularity advantageous, since TLR9 also localizes to endolysosomes. However, the loading capacity of CpG ODNs on the surface of BNNS was not sufficient to induce a robust cytokine response. In addition, a burst release of CpG ODNs from BNNS was observed. It is possible that these effects are due to the weak interaction between CpG ODNs and the surface of BNNS.

To ameliorate these problems, we screened peptides that have an affinity for BNNS and used the candidate peptide as a linker molecule to bind CpG ODNs to BNNS, which have a chemically inert and structurally stable surface.[30] Phage display has emerged recently as a powerful approach for identifying peptide motifs that possess high affinity and specificity against a particular target, including various inorganic nanomaterials,[32-33] metals,[34-36] semiconductors,[37-38] and polymers.[39]

Using this technique, we identified a peptide with selective affinity for BNNS, and characterized the intracellular delivery and response to CpG ODNs indirectly bound to BNNS through the linker peptide.

2. Materials and methods

2.1. Materials

Highly pure BNNS, with an average size of approximately 150 nm, were synthesized by a chemical vapor deposition method as previously reported.[30] Fluorescein isothiocyanate (FITC)-labeled peptides were purchased from Thermo Fisher Scientific (Germany). Phosphodiester-based class-B CpG ODNs, referred to as CpG ODN2006x3-PD,[40] were purchased from Fasmac, Inc. (Kanagawa, Japan). CpG ODNs were diluted in sterile water and stored at -20°C.

2.2. Screening of BNNS-binding peptides using phage display

BNNS (1 mg/mL) were suspended by sonication in Tris-HCl–buffered saline (50 mM HCl, 150 mM NaCl, pH 7.5) containing 0.1% Tween-20 (TBS-T). The Ph.D.-12 phage library (New England Biolabs, Beverly, MA, USA) containing 1×10^{11} pfu was added to 1 mL BNNS solution. After incubation for 1 h at room temperature with gentle agitation, the BNNS were washed 10 times with TBS-T to remove any unbound phages. Bound phages were then eluted by incubation for 10 min at room temperature in 1 mL of 0.2 M glycine-HCl (pH 2.2). The eluted phages were immediately neutralized by adding 150 µL of 1 M Tris-HCl (pH 9.1), and the number of phages was estimated by infecting *Escherichia coli* strain ER2738. The eluted phages were amplified in *E. coli* and subjected to the next round of panning, which was repeated 5 times. By the fifth panning, the phage recovery ratio (output phage:input phage) was high enough to pick 96 individual clones, which were then characterized by sequencing with the universal primer 96 g III (5′-3′CCCTCATAGTTAGCGTAACG) purchased from Fasmac, Inc. (Kanagawa, Japan)

2.3. Determination of peptide to BNNS affinity

FITC-labeled peptides were dissolved in TBS-T at 10 µg/mL. For direct binding studies, 500 µL of FITC-labeled peptide was added to an equal volume BNNS solution and incubated for 1 h at room temperature. The BNNS mixture was then washed 6 times with TBS-T to remove unbound phages. 10 µL of peptide-bound BNNS suspension was placed on a glass slide, visualized by fluorescence microscopy (DM2500, Leica, Germany), and quantified with Image J software (written by Wayne Rasband). Binding affinities are expressed as the average fluorescence intensity of the images. In the control group, the BNNS were incubated without peptides.

2.4. Determination of peptide to BNNS specificity

Five-hundred microliters of FITC-labeled BP1 or BP7 (1 μg/mL in TBS-T) were incubated with 500 μg of BNNS or other nanomaterials for 1 h with gentle rotation. The mixture was then centrifuged and the supernatant was collected. Fluorescence intensities (FI) of the supernatants were measured by a microplate reader (MTP-880 Lab, Corona). The binding specificity of BP1 and BP7 to each nanomaterial was calculated as the percentage of each peptide that bound to it.

2.5. Characterization of peptides and BNNS

Circular dichroism (CD) spectra were obtained using a J-725 spectrophotometer (JASCO, Japan) at room temperature. Fluorescence spectra were analyzed by a F-7000 spectrofluorometer (Hitachi, Japan) with an excitation of 260 nm and a scanning rate of 240 nm/min. UV/vis absorption spectra were measured with a U-2900 spectrophotometer (Hitachi, Japan) at room temperature. Zeta potential measurements were conducted using a LEZA-600 electrophoresis zeta potential analyzer (Otsuka, Japan).

2.6. Cell culture

HeLa cells, a cervical cancer–derived cell line, were maintained in Eagle's minimum essential medium (MEM) (Life Technologies, Carlsberg, CA, USA) containing 10% v/v fetal bovine serum (FBS) and penicillin/streptomycin (100 mg/L medium). HEK293XL/null cells, a human embryonic kidney cell line, were purchased from InvivoGen (San Diego, CA, USA) and grown in Dulbecco's modified Eagle medium (DMEM) (Sigma-Aldrich, St. Louis, MO, USA) containing 10% (v/v) FBS and penicillin/streptomycin (100 mg/L). Frozen peripheral blood mononuclear cells (PBMCs) were purchased from Cellular Technology Limited (Shaker Heights, OH, USA) and thawed according to the manufacturer's protocol. All cell lines were incubated at 37°C with 5% CO_2.

2.7. Cytotoxicity assay

Cytotoxicity of BNNS and the BNNS/BP7 complex was investigated using a water-soluble tetrazolium salt assay (CCK-8). A total of 4000 cells were seeded in a 96-well plate for 24 h to allow the cells to adhere, after which the cells were exposed to serial dilutions of BNNS, BNNS/BP7 complex, or medium (control). After a 24-h incubation at 37°C with 5% CO_2, 10 μL of CCK-8 solution was added to each well and incubated for another 3 h. Next, the absorbance was measured at a wavelength of 450 nm. Cytotoxicity was expressed as the percentage of cell viability compared to that of untreated control cells.

2.8. Cellular uptake

HeLa or HEK293XL/null cells (4×10^4) were seeded in a 35-mm petri dish with a glass bottom and incubated for 24 h at 37°C with 5% CO_2. BNNS/BP7 complex was then added to the dish at a

final concentration of 50 μg/mL. After incubation for 24 h, the cells were washed twice with PBS and fixed with 3.7% (v/v) paraformaldehyde. The fixed cells were visualized using confocal laser scanning microscopy (SP5; CLSM, Leica, Germany).

2.9. Preparation of BP7–CpG ODNs conjugates

BP7–CpG ODNs conjugates were prepared using a protein–protein crosslinking kit (Molecular Probes, Invitrogen, CA, USA) according to the manufacturer's instructions. Briefly, a thiol-reactive maleimide group was introduced on the lysine residue of BP7 by incubation with excess *trans*-4-(maleimidylmethyl)cyclohexane-1-carboxylate. The BP7-maleimide was then incubated with thiol-labeled CpG ODNs to form a stable thioester bond between BP7 and CpG ODNs. The conjugates were confirmed by native polyacrylamide gel electrophoresis and ethidium bromide staining.

2.10. CpG ODNs loading

CpG ODNs and BP7–CpG ODNs conjugates were incubated with 40 μL of BNNS solution (2 mg/mL in PBS at pH 7.4) at a final concentration of 100 ng/mL for 1 h, followed by centrifugation to remove unbound material in the supernatant. Supernatant CpG ODNs concentration was measured by a Nano Drop 2000 spectrophotometer (Thermo Scientific). Loading capacity was defined as the amount of CpG ODNs per 1 mg BNNS. The CpG ODNs and BP7–CpG ODNs conjugates–loaded BNNS were resuspended by adding 46 μL PBS and used for cytokine induction. The microstructures of the BP7–CpG ODNs conjugates–loaded BNNS were observed by 3000F high-resolution field emission transmission electron microscopy (JEOL, Japan) operated at an acceleration voltage of 300 kV.

2.11. CpG ODNs release assay

One milliliter PBS (adjusted to pH 5.0 with HCl) was added to 1 mg CpG ODNs or BP7–CpG ODNs conjugates–loaded BNNS and stirred at room temperature. At regular intervals, the solution was centrifuged, and aliquots of PBS (200 μL) were removed to measure the concentration of released CpG ODNs. A total of 200 μL fresh PBS was added to the solution for each aliquot removed.

2.12. Cytokine assay

PBMCs were seeded in RPMI 1640 medium supplemented with 10% FBS, at a density of 5×10^6 cells/mL. Cells were immediately stimulated with CpG ODNs or BP7–CpG ODNs conjugates–loaded BNNS. The final concentration of BNNS was about 87 μg/mL. Free BP7–CpG ODNs conjugates were used at a final concentration of 1 μg/mL, corresponding to the concentration

of the BNNS-loaded conjugates. After 24h and 8h of incubation respectively at 37°C, cell supernatants were collected for further analysis. The concentration of interleukin-6 (IL-6), tumor necrosis factor-alpha (TNF-α) and interferon-α (IFN-α) in the media was determined by enzyme-linked immunosorbent assay (ELISA) using the Ready-SET-Go! Human IL-6 kit (eBiosciences, CA, USA), Human TNF-α kit (eBiosciences, CA, USA) and Human IFN-alpha-Module set (eBioscience, Vienna, Austria), as per manufacturer's protocol.

2.13. Statistical analysis

Statistical analysis was performed using Student's *t*-test. Data are presented as mean ± SD. Differences were considered statistically significant for $*p < 0.05$ and $**p < 0.01$.

3. Results and discussion

3.1. Screening for BNNS-specific peptides

We used a randomized 12-mer peptide phage library (Ph.D.-12, New England Biolabs) commonly used for screening peptide aptamers against various targets. Phages were incubated with highly pure BNNS synthesized using chemical vapor deposition (**Fig. 1**). The ratio of output to input phages increased continuously for 5 rounds of panning against BNNS (**Supplementary Fig. 1**), demonstrating that phages with higher affinities had been successfully concentrated in the phage pool. We randomly picked 96 individual clones from the phage pool; DNA sequence analysis revealed that the clones consisted of 8 different peptides (**Table 1**). Of these clones, LLADTTHHRPWT (referred to as BP1), had the highest frequency (58%). Similar to carbon nanotube (CNT)-binding peptides reported previously,[41] the BNNS-binding peptides were significantly rich in aromatic residues, including histidine (H and tryptophan (W), compared to the original phage library (**Supplementary Fig. 2**). However, we could not find a consensus amino acid sequence or shared features in the selected peptides, suggesting that each peptide might have their own binding site and BNNS-binding mechanism.

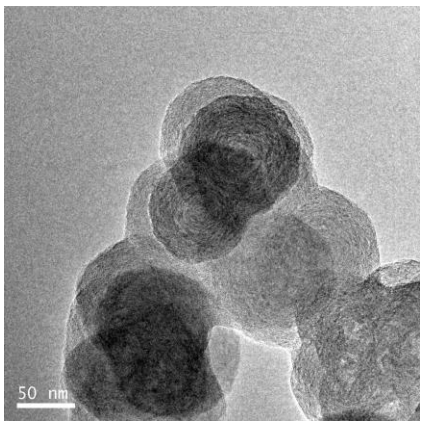

Fig. 1. Transmission electron microscopy image of boron nitride nanospheres (BNNS).

Table 1. Selected peptides with affinity for BNNS.

Name	Sequences	Frequency (%)	pI[a]
BP1	LLADTTHHRPWT	58.3	6.92
BP2	APLQPRSDNPFR	8.3	9.64
BP3	SATTPLIFPQTT	6.3	5.24
BP4	YPAPQPLVTKTS	6.3	8.59
BP5	ERSWTLDSALSM	5.2	4.37
BP6	QHSAAHYSTRLS	3.1	8.76
BP7	VDAQSKSYTLHD	3.1	5.39
BP8	SFHQLPARSPLP	2.1	9.49

[a] pI = isoelectric point. Values are calculated using online software (http://au.expasy.org/).

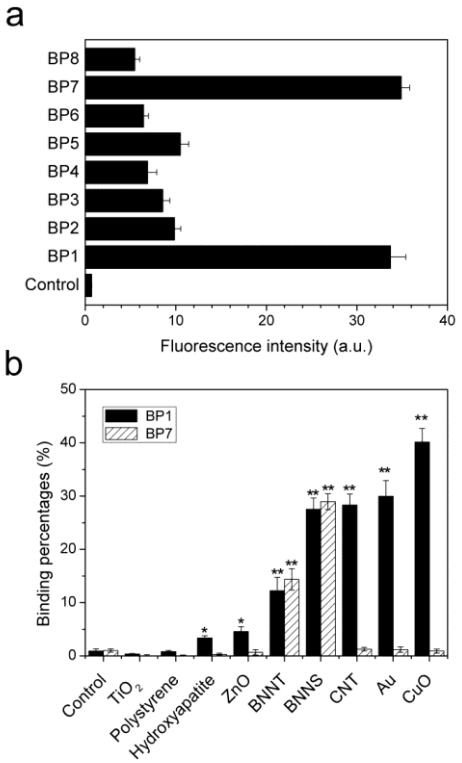

Fig. 2. BNNS binding affinity and specificity analysis of selected peptides. (a) Binding affinities of the peptides for BNNS. FITC-labeled peptide was incubated with BNNS for 1 h, washed, and visualized. Binding affinity was determined by averaging the fluorescence intensity of the images. (b) To determine binding specificities, FITC-labeled BP1 and BP7 were incubated with BNNS or other nanomaterials for 1 h. Solutions were centrifuged and unbound peptide was determined by the fluorescence intensity of supernatant. Binding specificities were calculated as the percentage of peptide that bound to each nanomaterial. Data are presented as mean ± SD (n = 3); $*p < 0.05$, $**p < 0.01$.

To further investigate the BNNS-binding affinities and specificities of the peptides, we labeled the peptides with fluorescein isothiocyanate (FITC). Fluorescent image analysis confirmed that all of the selected peptides bound to BNNS (**Fig. 2a, Supplementary Fig. 3**). Of them, 2 peptide sequences, LLADTTHHRPWT (BP1) and VDAQSKSYTLHD (BP7), showed a higher affinity for BNNS (**Fig. 2a, Supplementary Fig. 3**). We next examined the binding specificities of these 2 peptides with BNNS and 8 other types of nanomaterials. Although BP1 showed cross-affinity to various types of nanomaterials such as carbon nanotubes (CNT), gold (Au) nanoparticles, and copper oxide (CuO) nanoparticles, as observed by other researchers,[33, 41-42] BP7 specifically bound to BNNS (**Fig. 2b**). In addition, BP7 binding notably improved the solubility of BNNS in aqueous solution. The solubility and dispersion of BNNS are crucial characteristics for potential applications in drug delivery systems.

3.2. BP7 to BNNS binding properties

To identify key amino acid residues involved in the binding of BP7 to BNNS, we constructed a series of FITC-labeled BP7 variants in which specific amino acids were substituted by alanine (A) residues or terminal sequences were deleted. Replacing valine (V), tyrosine (Y), and leucine (L) at the first (V1), eighth (Y8), and tenth (L10) positions from the N-terminus of BP7 impaired BNNS binding (**Fig. 3**). In addition, the deletion of 3 residues from either terminus of BP7 also reduced the affinity. In particular, the mutation of tyrosine (Y8A) significantly affected the binding affinity for BNNS, suggesting that Y8 is essential for binding. Substitution of the remaining 4 amino acid residues with alanine (D2A, K6A, H11A, and D12A) had little effect on the binding. Tyrosine is an aromatic amino acid that is expected to form π–π interactions, while valine and leucine are nonpolar residues that easily form hydrophobic interactions. These interactions have been reported to be important for CNT and BN nanotubes (BNNT) binding peptides.[25, 32, 43]

To characterize the conformational features of BP7, we measured the CD spectrum of free BP7 in the presence and absence of BNNS. Molecular conformation plays an important role in determining the binding strength of peptides to a target.[43-44] As shown in **Fig. 4a**, BP7 had a peak at around 200 nm in solution, which is a typical random coil spectrum. However, the spectrum dramatically changed when bound to BNNS, suggesting a conformational change of BP7 on the surface of BNNS. Such a conformational change from a random coil is also reported in BP1 (also known as UW-1), which was identified as a binding peptide to single-walled CNT.[41] According to molecular dynamic simulation, peptides are believed to change their conformation and spatial arrangement on nanomaterials, depending on the surface energy of the nanomaterial and charge balance between peptide and material.[43]

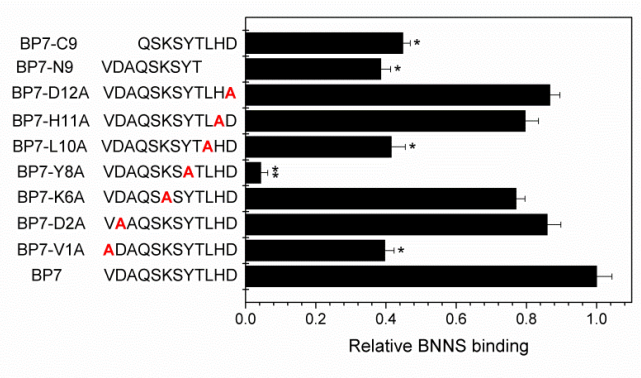

Fig. 3. Binding affinity of BP7 mutants for BNNS. Terminal sequence deletion and Ala scanning (i.e., the substitution of alanine residues (A) for amino acids within the peptide) were used to determine key amino acids for BP7 binding. Binding affinity was determined as previously described and normalized to BP7 binding. Data are presented as mean ± SD (n = 3). *$p < 0.05$, **$p < 0.01$.

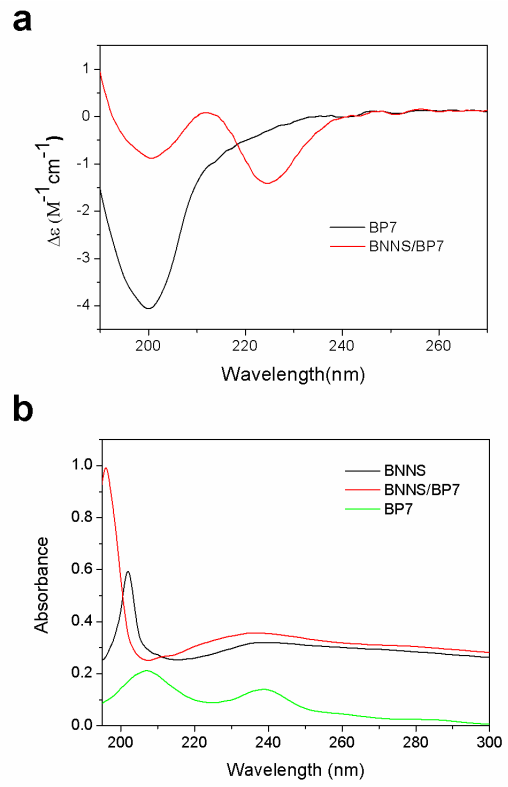

Fig. 4. Characterization of BP7 and BNNS. (a) CD spectra of BP7 and the BNNS/BP7 complex measured between 190 nm and 270 nm with a scanning speed of 20 nm/min and a bandwidth of 0.5 nm. (b) UV/vis absorption spectra of BNNS, BP7, and the BNNS/BP7 complex.

To gain further insight into the mechanism of the π–π interactions between BNNS and BP7, we investigated the fluorescence spectra of pure BNNS, pure BP7, and the BNNS/BP7 complex (**Supplementary Fig. 4**). The peak corresponding to tyrosine residues appeared at 313 nm in pure

BP7 and shifted to 328 nm in the BNNS/BP7 complex. This result implies that a charge transfer occurred between BNNS and BP7 due to the strong π–π interactions, similar to the CNT-binding peptide reported previously.[41] Such charge transfer is also observed between CNT and polymers.[45] The UV/vis absorption spectra showed that the sharp peak assigned to pure BNNS appeared at 202 nm and shifted to 196 nm in the BNNS/BP7 complex (**Fig. 4b**). This observation suggests that the electronic structure of BNNS was affected by the charge transfer between BNNS and BP7 from the π–π interaction. However, the detailed mechanisms of this π–π interaction remain unclear.

3.3. Cytotoxicity and cellular uptake of the BNNS/BP7 complex

Biological safety is a critical criterion in the application of nanomaterials as carriers for drug delivery.[46] Although BNNS and BNNT have been reported to be suitable materials for drug delivery, [27, 31] the safety of the BNNS/BP7 complex warranted investigation. Similar to BNNS, the BNNS/BP7 complex showed no apparent decrease in cellular viability of human PBMCs (**Fig. 5**), HeLa cells, or HEK293 cells (**Supplementary Fig. 5a**), even at a concentration of 100 μg/mL, suggesting no cytotoxic effect of BP7 on the safety of BNNS.

Cellular uptake is another important criterion for the application of nanomaterials as an intracellular delivery system. When cells were incubated for 24 h with 50 μg/mL BNNS loaded with FITC-labeled BP7, we observed intracellular FITC fluorescence (**Supplementary Fig. 5b**). This implies that BP7 was carried into the cells by BNNS. Moreover, compared to our previous cellular uptake investigation of the pure BNNS, no distinct enhancement by BP7 was obsversed in this study, both of the BNNS and the BNNS/BP7 complex showed good cellular uptake behavior. These results suggest that the BNNS/BP7 complex is an efficient carrier for intracellular delivery of CpG ODNs.

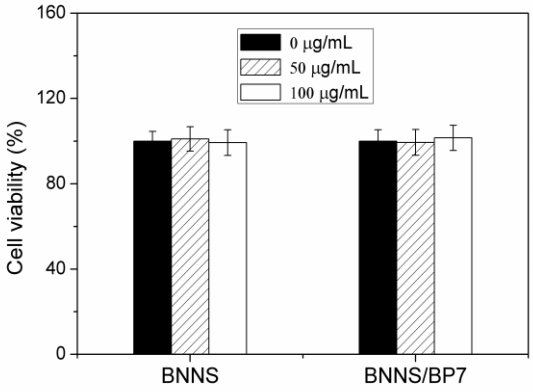

Fig. 5. Cytotoxicity of BNNS and the BNNS/BP7 complex. Peripheral blood mononuclear cells (PBMCs) were incubated with increasing concentrations of BNNS or the BNNS/BP7 complex, and cell viability was measured by a water-soluble tetrazolium salt assay. Data are presented as mean ± SD (n = 5).

3.4. Loading capacity of CpG ODNs on BNNS

We modified the lysine of BP7 with a thiol-reactive maleimide and thiolated the 3′ end of class-B CpG ODNs. The thiolated CpG ODNs were crosslinked with the maleimide-modified BP7, resulting in the formation of a BP7–CpG ODNs conjugates. The conjugates were then loaded on BNNS, with BP7 serving as a linker. The maximum loading capacity of CpG ODNs was dramatically increased when BP7 was used as a linker, to approximately 5-fold higher than CpG ODNs loaded directly onto BNNS (**Fig. 6a**). However, when we used another two BP7 mutants (BP7-Y8A and BP7-L10A) as linkers, which had the reduced affinity for BNNS, the loading capacity of their conjugates with CpG ODNs on BNNS significantly decreased compared to that of BP7 (**Supplementary Fig. 6**). These results suggest that the higher loading capacity of BP7–CpG ODNs is due to the high binding affinity of BP7 to BNNS. We then examined the morphology of BP7–CpG ODNs conjugates on BNNS using a transmission electron microscope (TEM). An amorphous-like layer was clearly observed on the surface of BNNS (**Fig. 6b**), indicating the bound BP7–CpG ODNs conjugates. However, the conjugates were not uniformly distributed on the surface. This irregular binding may be attributed to the heterogeneity of the BNNS surface. Oxygen impurities might affect the affinity of BP7–CpG ODNs for the surface of BNNS, due to the irregular distribution of oxygen impurities during the formation of BNNS.[30]

Next, we tested the release of the BP7–CpG ODNs conjugates from the surface of BNNS under acidic conditions that correspond to the physiological environment in a TLR9-localized endolysosome. Approximately 65% of CpG ODNs directly bound to BNNS was quickly released from BNNS within 12 h, while only 30% of the BP7–CpG ODNs conjugates were released within 24 h (**Fig. 6c**). After 48 h, almost no further release of the BP7–CpG ODNs conjugates could be obversed. This suggests CpG ODNs could not be easily released from BNNS surface because of the stronger binding of the BP7–CpG ODNs conjugates to BNNS than direct binding of CpG ODNs.

Zeta potential showed that BNNS have a slight negative surface charge density (**Supplementary Fig. 7**), suggesting that the lower loading capacity of negatively charged, free CpG ODNs may be due to the negative surface charge of BNNS. However, the BNNS/BP7 complex showed a higher negative charge density compared to BNNS (**Supplementary Fig. 7**), implying that BP7 also has a negative charge. This is in accordance with our theoretical prediction (**Table 1**), with BP7 having a predicted isoelectric point of 5.39. However, BP7 was still able to bind to the negatively charged BNNS, suggesting that the strong π–π interaction and hydrophobic interaction between BNNS and BP7 can overcome the electrostatic repulsion.

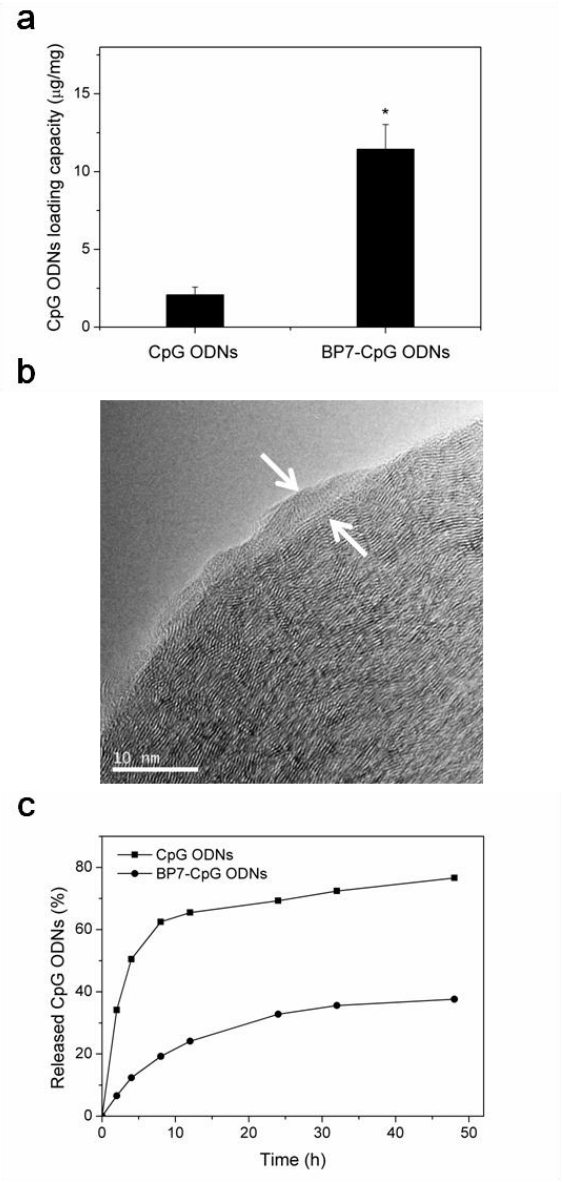

Fig. 6. Loading capacity and release properties of CpG oligonucleotides (CpG ODNs) on BNNS. (a) Loading capacity of CpG ODNs and the BP7–CpG ODN conjugate on BNNS, denoted as μg CpG ODNs loaded on 1 mg BNNS. (b) TEM image of BP7–CpG ODN conjugate–loaded BNNS. The white arrows indicate the bound layer of BP7–CpG ODNs. (c) Release profile of CpG ODNs and the BP7–CpG ODN conjugate loaded on BNNS at pH 5. Data presented as mean ± SD (n = 3); *$p < 0.05$.

3.5. Cytokine induction by BP7-CpG ODNs conjugates delivered by BNNS

Though the class-B CpG ODN used in this study activates TLR9 and induces IL-6 and TNF-α, it does not potently induce IFN-α to the extent of class-A CpG ODNs.[47-51] However, Kerkmann et al.

reported that class-B CpG ODNs loaded on cationic polystyrene nanoparticles with a diameter of 180 nm induced IFN-α to a greater degree than did free class-A CpG ODNs.[52]

The BP7–CpG ODNs induced IL-6 and TNF-α (**Fig. 7**), but not IFN-α (**Supplementary Fig. 8**). CpG ODNs loaded directly on BNNS induced about twice the amount of IL-6 and TNF-α than the free BP7–CpG ODN conjugate (**Fig. 7**). This was mainly due to the improved cellular uptake efficiency of CpG ODNs by the BNNS carrier. In our previous work, when fluorescein labeled free CpG ODNs was added to cultured 239XL-TLR9 cells, fluorescence was not observed inside the cells. In contrast, strong fluorescence was observed in CpG ODNs when delivered by BNNS.[31] As expected, BP7–CpG ODNs conjugates loaded BNNS induced the highest level of IL-6 and TNF-α (**Fig. 7**). However, when we used another two BP7 mutants (BP7-Y8A and BP7-L10A) –CpG ODNs conjugates loaded BNNS to stimulate the PBMCs, the level of IL-6 and TNF-α induction significantly decreased compared to that of BP7 (**Supplementary Fig. 9**). This indicates that the higher IL-6 and TNF-α induction of BP7–CpG ODNs conjugates loaded BNNS should be attributed to the higher loading capacity of BP7–CpG ODNs on BNNS.

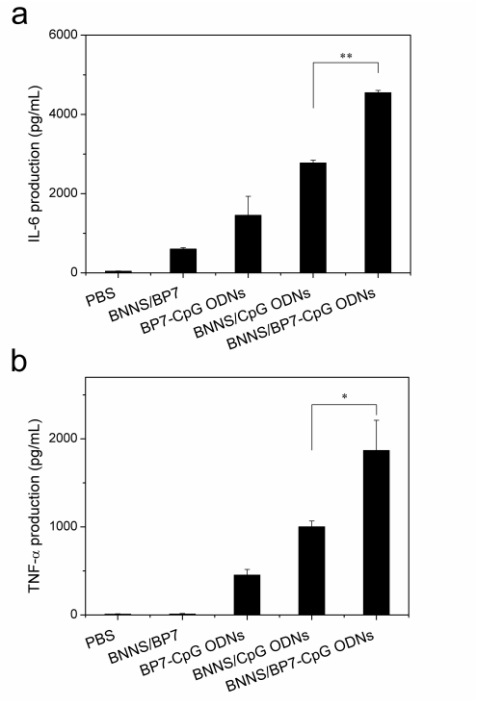

Fig. 7. Cytokine induction in PBMCs stimulated by BP7–CpG ODN conjugate–loaded BNNS. Loaded BNNS (87 μg/mL) or a corresponding concentration of free BP7–CpG ODN conjugate (1 μg/mL) was incubated with PBMCs for 8h (TNF-α) and 24h (IL-6) respectively. (a) IL-6 production. (b) TNF-α production. Data are presented as mean ± SD (n = 3); *$p < 0.05$, **$p < 0.01$.

IL-6 and TNF-α induction is thought to be mainly by BP7–CpG ODNs on BNNS, but not free BP7–CpG ODNs released from BNNS. BP7–CpG ODNs without BNNS and BP7–CpG ODNs

loaded on BNNS were used at the same concentration. Therefore, since only 30% of the BP7–CpG ODNs conjugates were released from BNNS within 24 h, IL-6 and TNF-α induction by released BP7-CpG ODNs alone would have resulted in less IL-6 and TNF-α than that induced by free BP7–CpG ODNs. Structure of the CpG ODNs plays an important role in their immunostimulatory effect.[53] Class A CpG ODNs induce the production of IFN-α, as they form a higher-order structures. However, such higher-order structures are not observed in class B CpG ODNs, they form a linear structures.[54] Although unmodified class-B CpG ODNs do not have the potential to induce IFN-α, it has been reported that class-B CpG ODNs electrostatically adsorped onto polystyrene and silica nanoparticles induce IFN-α.[52] However, BP7-CpG ODNs loaded on BNNS, like free CpG-ODNs, were not capable of inducing IFN-α. The polystyrene nanoparticles used in the studies had surfaces coated with cations for electrostatic binding of CpG ODNs.[52] Because of this, it is possible that all of the nucleotides in CpG ODNs bound to the cationic surface of the nanoparticles, since the negatively charged phosphate group of the nucleotides was involved in the electrostatic binding. In contrast, in BP7–CpG ODNs conjugates, only 1 terminus (3′ end) of a CpG ODN indirectly binds to the surface of BNNS through the linker peptide BP7, since the 3′ end of CpG ODN is thiolated for crosslinking with maleimide-modified BP7. Therefore, the method of binding for BP7–CpG ODNs on BNNS differs from CpG ODNs binding on polystyrene nanoparticles. This difference in binding method may affect the activation of TLR9 and further influence the potential for cytokine induction.

4. Conclusion

The peptide BP7 (VDAQSKSYTLHD) was identified from a combinatorial phage display library and was found to exhibit a highly specific binding to BNNS. The tyrosine residue (Y8) of BP7 was critical to maintain high affinity for BNNS. Attractive π–π interactions are considered to be the main driving force for the binding of BP7 to BNNS, although hydrophobic interactions may also be involved in the binding, which leads to a conformational change of BP7 on the surface of BNNS. The BNNS/BP7 complex was easily taken up by cells, and showed no cytotoxicity. By using BP7 as a linker molecule, BNNS were capable of delivering CpG ODNs to immune cells. BP7–CpG ODNs conjugates loaded on BNNS improved the capacity of IL-6 and TNF-α induction from PBMCs compared to that of CpG ODNs directly loaded on BNNS. The higher potential for cytokine induction in the BP7–CpG ODNs conjugates–loaded BNNS may be attributed to a higher loading capacity and stronger binding to BNNS. We anticipate that these findings will open a new avenue for the functionalization of BNNS with peptides and pave the way for the application of BNNS in the delivery of nucleic acid therapies, such as CpG ODNs and small interfering RNA.

Acknowledgements

This work was supported by a Grant-in-Aid for Scientific Research (C-22560777 and

23·01510) from the Japan Society for the Promotion of Science and the Ministry of Education, Culture, Sports, Science and Technology (MEXT).

Electronic supplementary information (ESI) available:

References

1. D. M. Klinman, *Nat. Rev. Immunol.*, 2004, **4**, 248-257.
2. H. Wagner, *Adv. Immunol.*, 1999, **73**, 329-368.
3. A. M. Krieg, A. K. Yi, S. Matson, T. J. Waldschmidt, G. A. Bishop, R. Teasdale, G. A. Koretzky and D. M. Klinman, *Nature*, 1995, **374**, 546-549.
4. J. Vollmer and A. M. Krieg, *Adv. Drug Delivery. Rev.*, 2009, **61**, 195-204.
5. H. Hemmi, O. Takeuchi, T. Kawai, T. Kaisho, S. Sato, H. Sanjo, M. Matsumoto, K. Hoshino, H. Wagner, K. Takeda and S. Akira, *Nature*, 2000, **408**, 740-745.
6. S. Bauer, C. J. Kirschning, H. Häcker, V. Redecke, S. Hausmann, S. Akira, H. Wagner and G. B. Lipford, *Proc. Natl. Acad. Sci. U. S. A.*, 2001, **98**, 9237-9242.
7. D. M. Klinman, A. K. Yi, S. L. Beaucage, J. Conover and A. M. Krieg, *Proc. Natl. Acad. Sci. U. S. A.*, 1996, **93**, 2879-2883.
8. A. M. Krieg, *Nat. Rev. Drug Discov.*, 2006, **5**, 471-484.
9. Y. M. Murad and T. M. Clay, *BioDrugs*, 2009, **23**, 361-375.
10. D. E. Fonseca and J. N. Kline, *Adv. Drug Delivery. Rev.*, 2009, **61**, 256-262.
11. D. M. Klinman, S. Klaschik, T. Sato and D. Tross, *Adv. Drug Delivery. Rev.*, 2009, **61**, 248-255.
12. S. Agrawal and Q. Y. Zhao, *Curr. Opin. Chem. Biol.*, 1998, **2**, 519-528.
13. G. K. Mutwiri, A. K. Nichani, S. Babiuk and L. A. Babiuk, *J. Controlled Release*, 2004, **97**, 1-17.
14. J. Kurreck, *Eur. J. Biochem.*, 2003, **270**, 1628-1644.
15. J. P. Sheehan and H. C. Lan, *Blood*, 1998, **92**, 1617-1625.
16. A. A. Levin, *Biochim. Biophys. Acta, Gene Struct. Expression*, 1999, **1489**, 69-84.
17. S. P. Henry, G. Beattie, G. Yeh, A. Chappel, P. Giclas, A. Mortari, M. A. Jagels, D. J. Kornbrust and A. A. Levin, *Int. Immunopharmacol.*, 2002, **2**, 1657-1666.
18. K. D. Wilson, S. D. de Jong and Y. K. Tam, *Adv. Drug Delivery. Rev.*, 2009, **61**, 233-242.
19. A. Bianco, J. Hoebeke, S. Godefroy, O. Chaloin, D. Pantarotto, J.-P. Briand, S. Muller, M. Prato and C. D. Partidos, *J. Am. Chem. Soc.*, 2004, **127**, 58-59.
20. S. M. Standley, I. Mende, S. L. Goh, Y. J. Kwon, T. T. Beaudette, E. G. Engleman and J. M. J. Fréchet, *Bioconjugate Chem.*, 2006, **18**, 77-83.
21. S. Rattanakiat, M. Nishikawa, H. Funabashi, D. Luo and Y. Takakura, *Biomaterials*, 2009, **30**, 5701-5706.
22. Y. Zhu, W. Meng, X. Li, H. Gao and N. Hanagata, *J. Phys. Chem. C*, 2010, **115**, 447-452.
23. N. G. Chopra, R. J. Luyken, K. Cherrey, V. H. Crespi, M. L. Cohen, S. G. Louie and A. Zettl, *Science*, 1995, **269**, 966-967.
24. C. Y. Zhi, Y. Bando, C. C. Tang, R. G. Xie, T. Sekiguchi and D. Golberg, *J. Am. Chem. Soc.*, 2005, **127**, 15996-15997.

25. Z. H. Gao, C. Y. Zhi, Y. Bando, D. Golberg and T. Serizawa, *J. Am. Chem. Soc.*, 2010, **132**, 4976-4977.
26. D. Golberg, Y. Bando, C. C. Tang and C. Y. Zhi, *Adv. Mater.*, 2007, **19**, 2413-2432.
27. X. Chen, P. Wu, M. Rousseas, D. Okawa, Z. Gartner, A. Zettl and C. R. Bertozzi, *J. Am. Chem. Soc.*, 2009, **131**, 890-891.
28. E. Jonsson, L. Simonsen, M. Karlsson and R. Larsson, *Ann. Oncol.*, 1998, **9**, 44-44.
29. R. S. Waritz, B. Ballantyne and J. J. Clary, *J. Appl. Toxicol.*, 1998, **18**, 215-223.
30. C. C. Tang, Y. Bando, Y. Huang, C. Y. Zhi and D. Golberg, *Adv. Funct. Mater.*, 2008, **18**, 3653-3661.
31. C. Y. Zhi, W. J. Meng, T. Yamazaki, Y. Bando, D. Golberg, C. C. Tang and N. Hanagata, *J. Mater. Chem.*, 2011, **21**, 5219-5222.
32. S. Q. Wang, E. S. Humphreys, S. Y. Chung, D. F. Delduco, S. R. Lustig, H. Wang, K. N. Parker, N. W. Rizzo, S. Subramoney, Y. M. Chiang and A. Jagota, *Nat. Mater.*, 2003, **2**, 196-200.
33. M. D. Roy, S. K. Stanley, E. J. Amis and M. L. Becker, *Adv. Mater.*, 2008, **20**, 1830-1836.
34. K.-I. Sano and K. Shiba, *J. Am. Chem. Soc.*, 2003, **125**, 14234-14235.
35. M. Sarikaya, C. Tamerler, A. K. Y. Jen, K. Schulten and F. Baneyx, *Nat. Mater.*, 2003, **2**, 577-585.
36. Y. Cui, S. N. Kim, S. E. Jones, L. L. Wissler, R. R. Naik and M. C. McAlpine, *Nano Lett.*, 2010, **10**, 4559-4565.
37. K. Goede, P. Busch and M. Grundmann, *Nano Lett.*, 2004, **4**, 2115-2120.
38. S. R. Whaley, D. S. English, E. L. Hu, P. F. Barbara and A. M. Belcher, *Nature*, 2000, **405**, 665-668.
39. T. Serizawa, T. Sawada and H. Matsuno, *Langmuir*, 2007, **23**, 11127-11133.
40. W. J. Meng, T. Yamazaki, Y. Nishida and N. Hanagata, *BMC Biotechnol.*, 2011, **11**.
41. Z. D. Su, T. Leung and J. F. Honek, *J. Phys. Chem. B*, 2006, **110**, 23623-23627.
42. H. Ejima, H. Matsuno and T. Serizawa, *Langmuir*, 2010, **26**, 17278-17285.
43. J. M. Slocik and R. R. Naik, *Chem. Soc. Rev.*, 2010, **39**, 3454-3463.
44. M. Hnilova, E. E. Oren, U. O. S. Seker, B. R. Wilson, S. Collino, J. S. Evans, C. Tamerler and M. Sarikaya, *Langmuir*, 2008, **24**, 12440-12445.
45. J. Chen, H. Liu, W. A. Weimer, M. D. Halls, D. H. Waldeck and G. C. Walker, *J. Am. Chem. Soc.*, 2002, **124**, 9034-9035.
46. Y. F. Zhu, T. Ikoma, N. Hanagata and S. Kaskel, *Small*, 2010, **6**, 471-478.
47. A. M. Krieg, *Annu. Rev. Immunol.*, 2002, **20**, 709-760.
48. M. Gursel, D. Verthelyi, I. Gursel, K. J. Ishii and D. M. Klinman, *J. Leukocyte Biol.*, 2002, **71**, 813-820.
49. G. Hartmann and A. M. Krieg, *J. Immunol.*, 2000, **164**, 944-952.

50. G. Hartmann, R. D. Weeratna, Z. K. Ballas, P. Payette, S. Blackwell, I. Suparto, W. L. Rasmussen, M. Waldschmidt, D. Sajuthi, R. H. Purcell, H. L. Davis and A. M. Krieg, *J. Immunol.*, 2000, **164**, 1617-1624.
51. A. Krug, A. Towarowski, S. Britsch, S. Rothenfusser, V. Hornung, R. Bals, T. Giese, H. Engelmann, S. Endres, A. M. Krieg and G. Hartmann, *Eur. J. Immunol.*, 2001, **31**, 3026-3037.
52. M. Kerkmann, L. T. Costa, C. Richter, S. Rothenfusser, J. Battiany, V. Hornung, J. Johnson, S. Englert, T. Ketterer, W. Heckl, S. Thalhammer, S. Endres and G. Hartmann, *J. Biol. Chem.*, 2005, **280**, 8086-8093.
53. N. Hanagata, *Int. J. Nanomedicine*, 2012, **7**, 2181-2195.
54. D. C. G. Klein, E. Latz, T. Espevik and B. T. Stokke, *Ultramicroscopy*, 2010, **110**, 689-693.

Table of contents

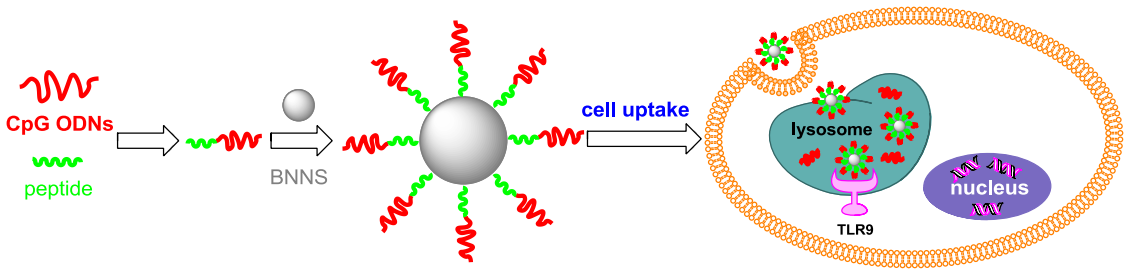

Using a boron nitride nanosphere (BNNS)-binding peptide as a linker molecule, BNNS are able to efficiently deliver immunostimulatory CpG ODNs into cells and significantly enhance the immune response.